International Conference on Space Optics—ICSO 2018

Chania, Greece

9–12 October 2018

Edited by Zoran Sodnik, Nikos Karafolas, and Bruno Cugny

Optical design and performance analysis of a CubeSat-sized limb sounder utilizing a spatial heterodyne spectrometer for the measurement of mesospheric temperature

Martin Kaufmann

Friedhelm Olschewski

Klaus Mantel

Oliver Wroblowski

et al.

International Conference on Space Optics — ICSO 2018, edited by Zoran Sodnik, Nikos Karafolas, Bruno Cugny, Proc. of SPIE Vol. 11180, 111803P · © 2018 ESA and CNES · CCC code: 0277-786X/18/$18 · doi: 10.1117/12.2536052

Optical design and performance analysis of a CubeSat-sized limb sounder utilizing a spatial heterodyne spectrometer for the measurement of mesospheric temperature

Martin Kaufmann*[a,b], Friedhelm Olschewski[b], Klaus Mantel[c], Oliver Wroblowski[a], Jilin Liu[a], Michael Deiml[aε], Qiuyu Chen[a], Ulrike Lembke[d], Saroj Mihalik[d], Brian Solheim[e], Gordon Shepherd[e], Ralf Koppmann[b], Martin Riese[a,b]

[a]Institute of Energy and Climate Research, Forschungszentrum Jülich, 52425 Jülich, Germany; [b]Institute for Atmospheric and Environmental Research, University of Wuppertal, Gausstr. 20, 42119 Wuppertal, Germany; [c]Max Planck Institute for the Science of Light, Staudtstr. 7/B2, 91058 Erlangen, Germany; [d]Mechatronics & Optics Division, European Space Research and Technology Centre, Keplerlaan 1, 2200 AG Noordwijk, The Netherlands; [e]Centre for Research in Earth and Space Science, York University, 4700 Keele Street, Toronto, Ontario, Canada; [ε]now at OHB System AG, Universitätsallee 27, 28359 Bremen Germany

ABSTRACT

A highly miniaturized limb sounder for the observation of the O_2 A-band to derive temperatures in the mesosphere and lower thermosphere is presented. The instrument consists of a monolithic spatial heterodyne spectrometer, which is able to resolve the rotational structure of that band. The SHS operates at a Littrow wavelength of 762 nm with a resolving power in the order of 10.000. Complemented by a front optics with an acceptance angle of less than ±1 degree and a detector optics, the entire optical system fits into a volume of about 1.5 liters. This allows this instrument to be flown on a three or six unit CubeSat. In this paper, we introduce the optical design and computer simulations on the expected performance of the instrument. The laboratory characterization of a prototype instrument, which has been built on university level, and the lessons learned are discussed.

Keywords: Spatial heterodyne spectrometer (SHS), limb sounding of the atmosphere, temperature measurement, CubeSat payload

1. INTRODUCTION

For the study of faint signals, Fourier Transform Spectrometers (FTS) have significant advantages over conventional grating spectrometers. Their performance (throughput or etendue) is typically more than two orders of magnitude larger than grating spectrometers of the same size. A Spatial Heterodyne Spectrometer (SHS) is a special type of a FTS. It has no moving parts and can be built as a monolithic structure. Combined with 2-dimensional imaging detectors, it records the interferogram of the scene in one dimension and spatial information in the second dimension.

A group of German and Canadian research institutes and universities started an initiative to develop SHS instruments for remote sounding of the Earth atmosphere. Several instruments measuring in the ultraviolet, visible, or shortwave infrared are currently under development.

This manuscript presents the basic design of an instrument to measure temperature in the mesosphere and lower thermosphere, calculations on the expected performance, and laboratory measurements. The instrument measures temperature by the evaluation of the rotational distribution of the O_2 (0,0) atmospheric A-band at 762 nm [1, 2, 3, 4, 5]. The emitting states have a lifetime of 12s, which is sufficiently long-lived to assure that the rotational distribution can be described by the kinetic temperature. The temperature derivation relies on the relative distribution of the emission lines

and does not require an in-orbit radiometric calibration. The use of silicon-based detectors operating at ambient or moderately cooled conditions reduces the power consumption, mass, and costs of such an instrument.

2. TEMPERATURE MEASUREMENTS BY MEANS OF O_2 A-BAND OBSERVATIONS

Light emitted in the O_2 atmospheric band system stems from emissions of the $O_2(b^1\Sigma_g^+)$ electronically excited state. An overview of the chemistry and molecular dynamics of excited O_2 is given by, e.g., [5] and references cited therein. All excitation processes of $O_2(b^1\Sigma_g^+)$ except one require sunlight. The only nighttime excitation process is chemiluminescence called the 2-step Barth process [21, 22]. There are three absorption bands in this system (A, B, and γ bands). All of these bands end up in a vibrational ground state. None of these bands can be observed from the ground, because of the high abundance of ground state molecular oxygen molecules in the atmosphere.
The spectral shape of the A-band around 762 nm for two different temperatures (for 200 K and 210 K) is illustrated in Figure 1. The spectra in the upper panel have been normalized to show identical band intensities. The light gray area shows their intensities (multiplied by a factor of 10) as seen from an instrument with a spectral resolution of 0.1 nm. The dashed line is the filter transmission curve of the instrument presented later. The dotted vertical line is drawn at the Littrow wavelength. The percentage difference of the line intensities are shown in the lower panel; the symbol size scales with the absolute intensity of the lines. It is clearly visible from the figure that higher temperatures give a flatter spectrum. A 10 K change in temperature affects the rotational distribution of strong emission lines at 760-765 nm between ±6%. This means that the band structure must be measured better than 1% to derive temperatures with a precision of 1.5 K.

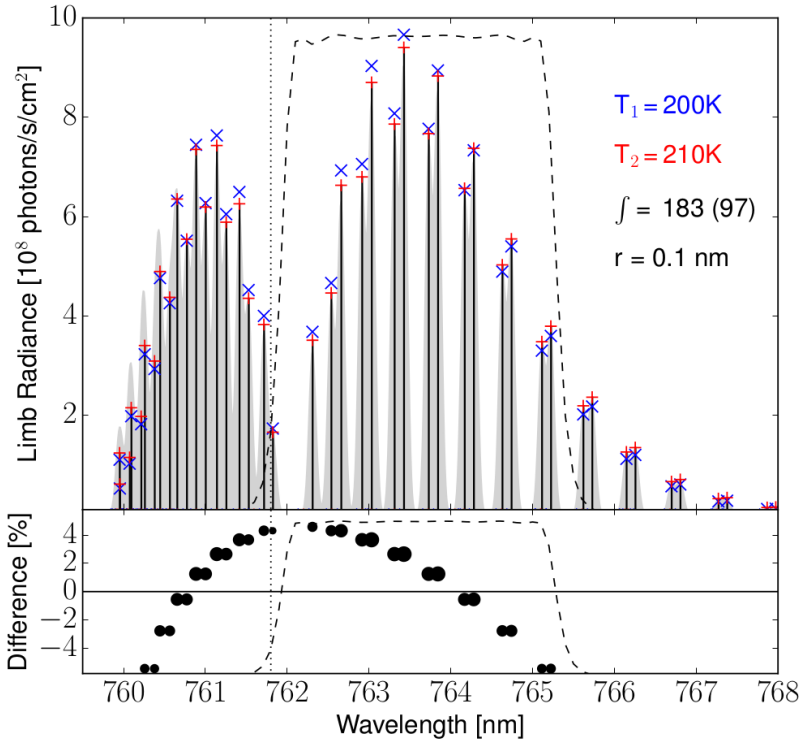

Figure 1. Typical O_2 A-band limb emission line calculations for nighttime conditions assuming a global temperature of 200 K and 210 K (upper panel). The percentage difference of the line intensities at 200~K and 210~K are shown in the lower panel

3. BASIC THEORY OF SPATIAL HETERODYNE SPECTROMETERS

In principle an SHS is a FTS, where the mirrors in each arm are replaced by diffraction gratings (Figure 2). The incoming wavefront is separated at the beamsplitter and diffracted at the gratings, with a wavelength-dependent angle. The superposition of the two wavefronts then produces straight, parallel, and equidistant fringes with a spatial frequency depending on the wavelength of the light. The zero frequency of the fringe pattern is at the Littrow wavelength and small wavenumber changes result in fringes with discernable, low spatial frequency, which can be observed with available imaging detectors. The concept was originally proposed by Pierre Connes in a configuration called "Spectromètre interférential à selection par l'amplitude de modulation (SISAM)" [7]. With the advent of imaging detectors, this idea was taken up by, e.g., [8, 9, 10, 11, 12, 13, 14, 15, 16, 17]. The design of an SHS for a particular wavelength range and desired spectral resolution follows a few simple relations, which are shortly summarized to illustrate the main characteristics of this device. For a derivation of the mathematical expressions see, e.g., [18, 19, 10], and references cited therein.

The tilt angle of the gratings with respect to the optical axis is called Littrow angle Θ_L. Light at the Littrow wavenumber σ_L is returned in the same direction as the incoming path, as described by the grating equation (for diffraction order one and grating groove density 1/d):

$$\sigma_L = \frac{1}{2d \sin \Theta_L}$$

Combining the intensity equation of a conventional FTS and the grating equation for small incident angles at the grating gives the SHS equation for ideal conditions, relating the incoming radiation at wavenumber σ to the spectral density at position x parallel to the dispersion plane. The heterodyned fringe frequency κ is:

$$\kappa = 4 \tan \Theta_L (\sigma - \sigma_L)$$

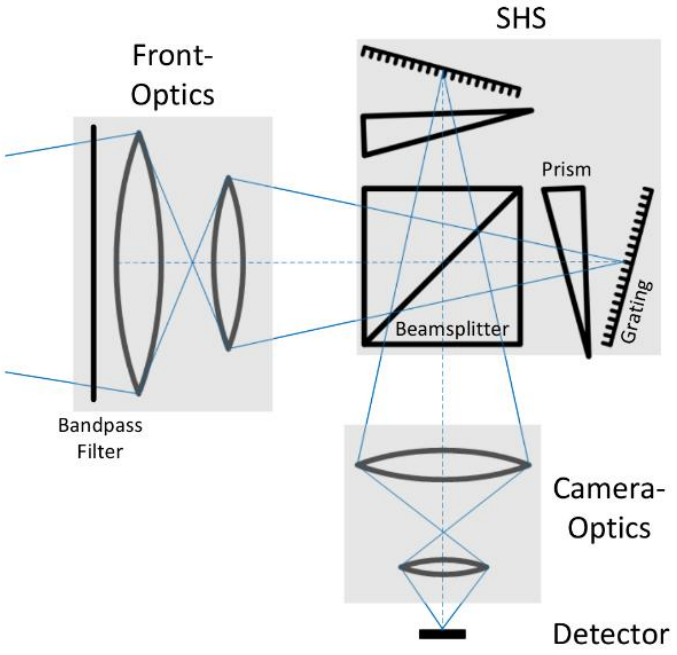

Figure 2. Principle design of the SHS with front and detector optics

The maximum resolving power of an SHS is nearly proportional to the number of grating grooves illuminated by the incoming beam. The bandwidth of an SHS is limited by the number of detector pixel due to the Nyquist theorem.

As for conventional FTS or Fabry-Perot instruments, the acceptance angle of light for a conventional SHS is inversely proportional to its resolving power [18]. The angle can be increased significantly, if prisms are inserted into the two interferometer arms. The prisms rotate the image of the gratings so that they appear to be located in a common virtual plane which is oriented perpendicular to the optical axis for a wide range of incident angles. At the end, the acceptance angle of the SHS including field widening prisms is only limited by spherical aberration for systems with small Littrow angles and astigmatism for large Littrow angles [20]. Depending on the actual design, the prisms increase the etendue or throughput of an SHS by 1-2 orders of magnitude.

A general advantage of SHS are the relaxed alignment tolerances, because in most optical setups the gratings are imaged onto a focal plane array. As a result, each detector pixel sees only a small area of the optical elements, so that moderate misalignments or inaccuracies in the surface quality affect limited spatial regions on the detector, only. This means that the interferogram is distorted locally rather than reduced in contrast. SHS can be realized using transmitting or all-reflecting elements. SHS using dispersive elements can be built monolithically, making them very robust for harsh environments, e.g. during rocket launches.

4. DESIGN PARAMETERS OF THE SHS LIMB SOUNDER FOR THE OBSERVATION OF O_2 A-BAND EMISSSIONS IN THE MESOPAUSE REGION

The goal was to design an SHS limb sounder to measure a section of the O_2 A-band spectrum at 762 nm. The requirements on the spectral resolution and the spectral bandpass were determined by simulation studies optimizing the retrieved atmospheric temperature accuracy and precision. Boundary conditions are the size of the instrument (shall fit into a volume of 1-2 litres excluding a straylight baffle), the usage of as many commercial off the shelf (COTS) components as possible, the detector size and pixel number (full HD, 5 um pitch), and a full field of view of 1.3°.

An integral part of an SHS design is the optical filter located between the SHS and the scene to be observed. For this instrument, a six cavity design bandpass filter with a center wavelength of 763.6 nm and a bandwidth of 3.4 nm was chosen. Since an SHS instrument maps the spectrum on both sides of the Littrow wavelength symmetrically into Fourier space, the filter must be adapted in such a way that there is no overlap of lines from different sides of the Littrow wavelength in the interferogram. In our design, the Littrow wavelength is at 761.8 nm, e.g. the filter blocks most of the radiance from the shorter wavelength side of the Littrow wavelength. The purpose of the front optics is to image a scene at the Earth's limb onto the gratings. The detector optics images the gratings onto the focal plane of the 2-dimensional detector. The image at the detector contains spatial information about the scene in both dimensions. An interferogram is superimposed on this scene in the direction perpendicular to the grating grooves. For the instrument presented in this work, the gratings are oriented in such a way that the interferogram spans over the horizontal direction, assuming that intensity fluctuations in the horizontal direction are small or smeared out during the exposure of the image compared to the modulation depth of the interferogram, which is valid in atmospheric limb sounding.

The basic design parameters of the SHS were calculated analytically using the SHS equations mentioned above. The materials of the optical glass components, the apex angle of the prisms as well as the distances between the various components were optimized and iterated by means of optical ray tracing software. The resulting basic design parameters are summarized in Table 1.

Table 1. Summary of optics, SHS and detector properties

attribute	property
front optics (incl. filter)	
wavelength range	761.9–765.3 nm
clear aperture diameter	66 mm
field of view	$\pm 0.65^o$
etendue (clear circular aperture)	0.014 cm^2 sr
focal length	136 mm
rectangular image size	$(3.8 \text{ mm})^2$
etendue (rectangular image)	0.01 cm^2 sr
SHS	
grating groove density	1200 lines/mm
Littrow wavelength	761.8 nm
Littrow angle	27.2^o
field of view	$\pm 5^o$
detector optics	
numerical aperture (obj. space)	0.12
magnification	0.55
focal length	28 mm
length of imaging system (incl. SHS)	75 mm
detector	
total pixel count	1920 x 1080
pixel size	5.04 x 5.04 μm^2
quantum efficiency	0.4 at 760 nm
dark current per pixel at 20^oC	2-4 e^-/s
readout noise (rms)	1 e^-
performance	
optical resolving power	16,800
expected resolving power (approx.)	8,000

The front optics (Figure 3) consists of four lenses, which image an object at infinity of an angular extent of 1.3° onto a circle of a diameter of 7 mm on the virtual image of the gratings. This corresponds to a theoretical spectral resolution of about 16,800. The clear aperture diameter of the front lens is 66 mm and the distance between the first lens and the SHS is 104 mm. The etendue of this configuration is 0.014 cm^2 sr. The detector optics images the active area of the gratings onto the detector and consists of four lenses as well. The magnification is 0.55, i.e. the illuminated area at the detector has a diameter of about 3.8 mm. This value was chosen as a trade-off between the form factor required and the desired spectral and spatial resolution. The distance between the beam splitter and the detector focal plane is 46 mm.

The detector chosen for this instrument is a low noise silicon-based CMOS image sensor. The optical format is 2/3 (9.7 mm x 5.4 mm) and the pixel size is 5.04 µm x 5.04 µm, resulting in 1920 x 1080 pixels in total, from those 840 x 840 pixels are used here. The quantum efficiency of this detector is about 0.4 at 760 nm.

Like the SHS, the entire optical system was optimized using optical raytracing software. The wave front peak-to-valley extension of the optical system is less than a half wavelength for center rays and one wavelength at maximum for the edge region of the field. The extension of the point spread function is 5 µm for inner and 10 µm for outer pixels, which does not deteriorate the determination of the different waves in the interferogram, because the highest spatial frequency to be observed corresponds to a wavelength of about 45 µm in the detector plane.

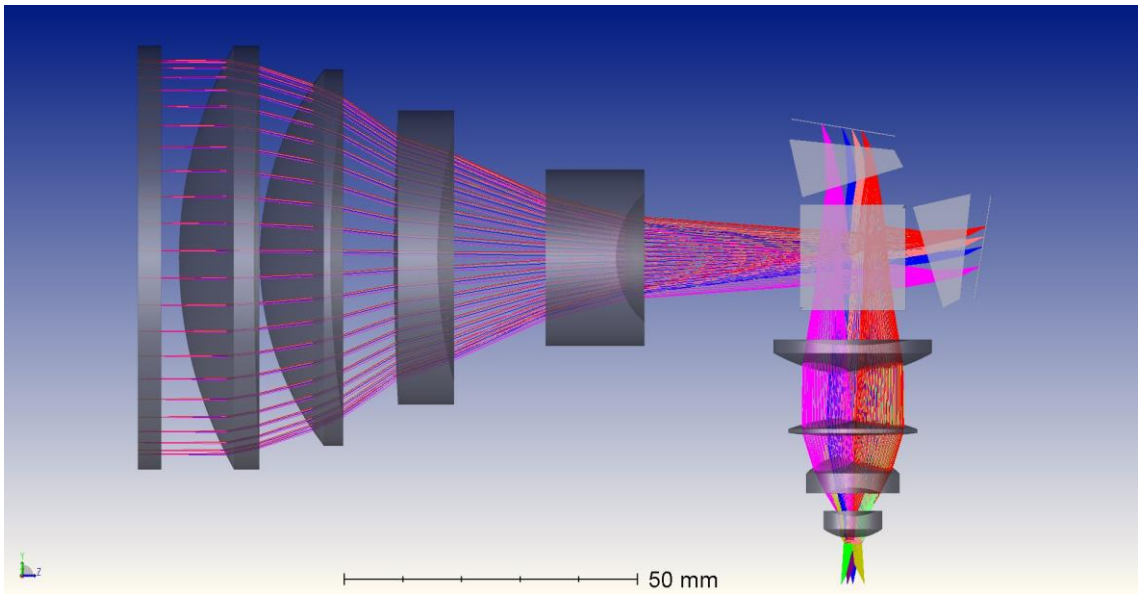

Figure 3. Optical components of the instrument, including the interference filter, the front optics, the SHS, the detector optics and the detector.

5. ASSEMBLY AND LABORATORY CHARACTERIZATION

The assembly of the SHS is performed by using optical glue. A picture of the assembled SHS is shown in Figure 4. The thickness of the glue is visually controlled, which requires interferometric control to assure that the designed Littrow wavelength is met. The visibility ν, which is defined as

$$\nu = \frac{I_{\max} - I_{\min}}{I_{\max} + I_{\min}}$$

and the tilt of the interferogram (which should be as low as possible) are optimized during the assembly procedure. For this SHS, a tunable external cavity diode laser is used to give the reference wavelength. The final configuration is a trade-off between the actual Littrow wavelength and the other figures of merit, while small deviations from the Littrow wavelength are acceptable, if the visibility and the spatial frequency keep within a given range and an overlap of lines from different sides of the Littrow wavelength is not critical.

The actual Littrow wavelength of the final assembly can be verified using the linear relation between the wavenumber (in cm^{-1}) and the spatial frequency of the interferogram by adjusting multiple laser wavelengths and measuring their corresponding spatial frequencies in the interferogram (Figure 5). For this SHS, the actual Littrow wavelength is 761.5 nm. Since the space between the beamsplitter, the prisms, and the gratings is filled with air and its refractive index is pressure dependent, the corresponding Littrow wavelength for vacuum conditions is shifted about 0.1 nm towards shorter wavelengths.

The visibility of the SHS within the optical system is about 80% in the center of the image and about 60% in the edge regions of the center line (Figure 6). The decrease towards the edges coincides with a similar decrease of the modulation transfer function (MTF).

Figure 4. Assembled SHS (38 x 38 x 27 mm^3)

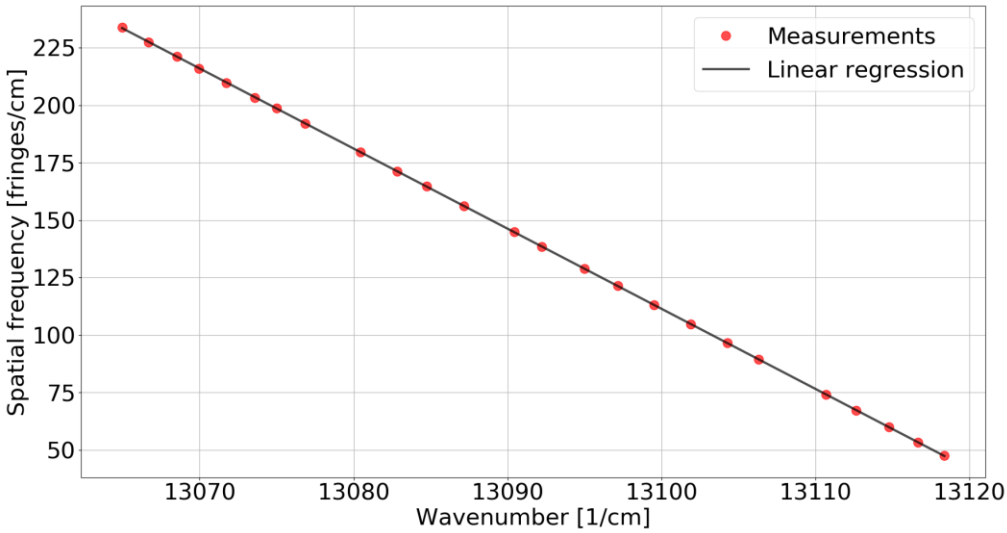

Figure 5. Spatial frequency of the interferogram depending on laser wavelength. The data is for laboratory conditions. The zero crossing is at 13132 cm^{-1} or 761.5 nm.

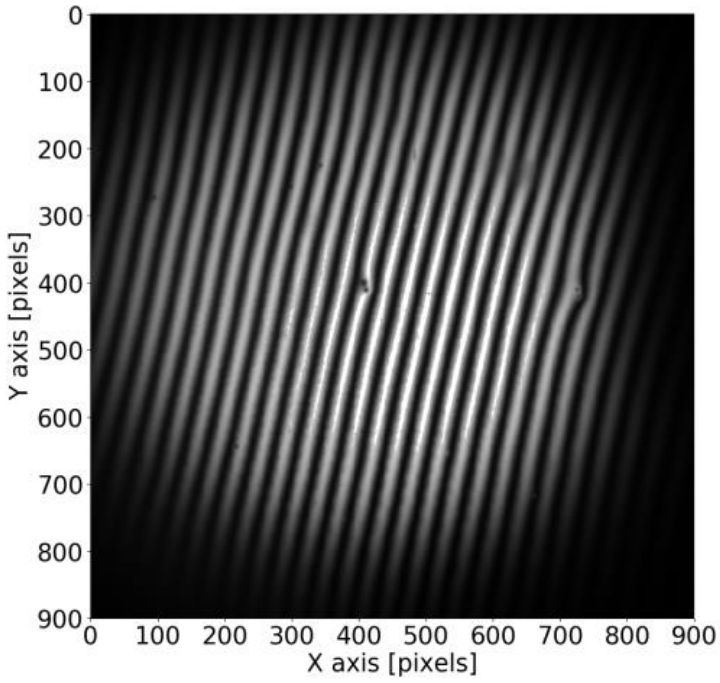

Figure 6. Interferogram of a laser line at 762 .5 nm

The slight tilt of the interferogram (4.3°) can be explained by a rotation of 0.01° of one grating to the other, caused by inaccuracies in the assembly procedure. The interferogram tilt depends on wavelength and varies between 8° at the short-wavelength edge (762.5 nm) of our region of interest and <2° at the long-wavelength edge (764.5 nm). It is evident that this tilt cannot be removed by image rotation due to its wavelength dependency and the related smearing in the vertical. However it is sufficiently small to introduce no significant loss of visibility (<2%), if 20 detector pixel rows are averaged to obtain the required signal-to-noise ratio. This averaging leads to a vertical sampling rate of about 1.4 km, since one detector row measures radiation from a 70 m thick tangent layer (for a typical 500 km low Earth orbit).

The spatial resolution of the instrument and the potential existence of optical ghosts was verified by simulations of the point spread function (PSF) and corresponding measurements. The simulated PSF for a perfectly aligned system is shown in Figure 7. It is almost the same for field angles between 0° and 0.35°, but starts to broaden for larger angles. For 0.65°, its width is 12µm corresponding to 160m at the Earth limb, which is acceptable compared to the nominal spatial resolution of 1.5km.

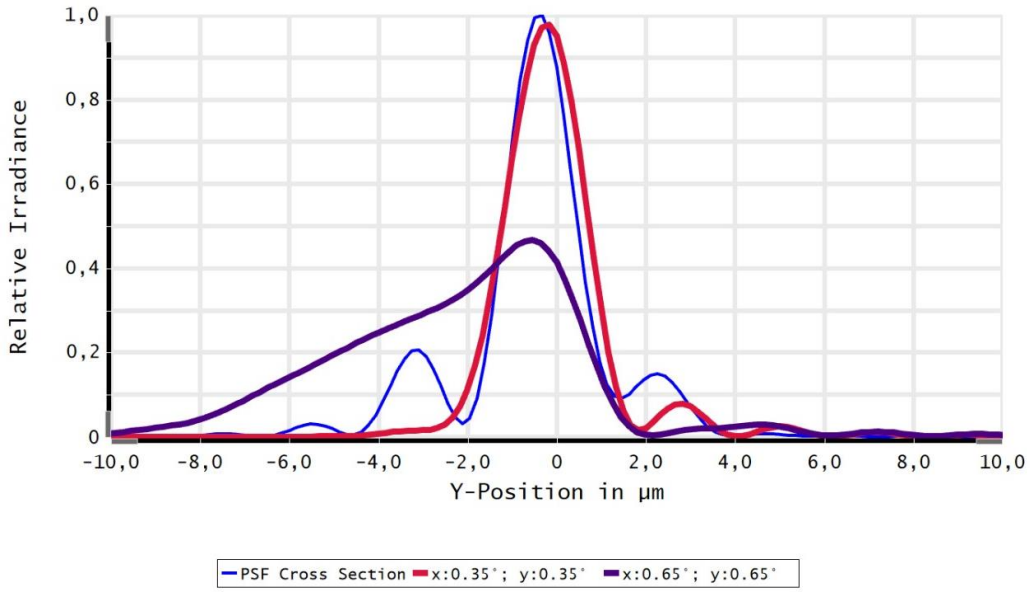

Figure 7. Calculated PSF, plotted in the direction perpendicular to the grating grooves, yielding the PSF extent in spectral direction. The curves are for different field angles.

To verify the PSF by measurement, a point-like source object was observed. This was realized by placing a pinhole with a diameter of 20 µm into the focal plane of a concave lens. Illumination of the pinhole with laser light at 762 nm wavelength resulted in plane waves with an angular extension of ±0.003°. By tilting the instrument in x-/y-directions, measurements at different field angles were obtained. A typical spot for on-axis rays is shown in Figure 8, which agreed well with simulations.

The pinhole measurements revealed the existence of optical ghosts, which are caused by internal reflections and appear as additional light spots on the focal plane. None of these ghosts showed intensities of more than 0.3% when compared to the main spot (PSF measurement). Simulations and measurements indicated that specular ghosts do not show fringe patterns. Therefore we expect their contribution to appear as low spatial frequency component/ spectral noise, which is not critical.

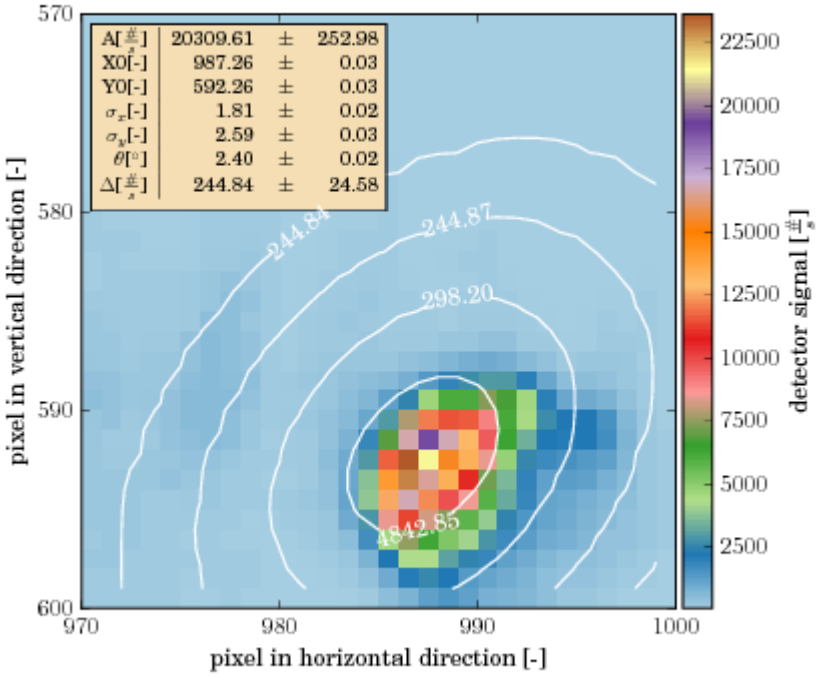

Figure 8. PSF measurements for a 20µm pinhole. on-axis. A two-dimensional Gaussian curve was fitted to evaluate position and extension of observed peaks. Fit parameters are given in the orange box in detector units (pixel, counts per pixel per second). The contour lines indicate the first four 1σ intervals.

6. CONCLUSIONS

A novel limb sounder for temperature sounding in the middle atmosphere is presented. Temperature is obtained from the measurement of the rotational structure of the O_2 A-band at 762 nm. The optical system consist of a spatial heterodyne spectrometer complemented by front- and detector optics. The size of the entire instrument including a straylight baffle is around 3.5 litres, and the power consumption is about 6 W. The instrument can deliver temperatures at a 2 K precision with an integration time of about one minute for nighttime and a few seconds for daytime conditions.

The instrument was designed and built to provide an inexpensive device for future nano-satellite constellations. The goal is to meet the performance of existing larger instruments. Preliminary analyses indicate that the design specifications are met.

REFERENCES

[1] R. Rodrigo, J. Lopez-Moreno, M. Lopez-Puertas, and A. Molina, "Analysis of OI-557.7 nm, NAD, OH(6-2) and $O_2(^1\varepsilon_g^+)$ (0-1) nightglow emission from ground-based observations," *Journal of Atmospheric and Terrestrial Physics*, vol. 47, no. 11, pp. 1099–1110, 1985.

[2] M. R. Torr, D. G. Torr, and R. R. Laher, "The O_2 atmospheric 0-0 band and related emissions at night from Spacelab 1," *Journal of Geophysical Research: Space Physics*, vol. 90, no. A9, pp. 8525–8538, 1985.

[3] I. C. McDade and E. J. Llewellyn, "The excitation of $O(^1S)$ and O_2 bands in the nightglow: a brief review and preview," *Canadian Journal of Physics*, vol. 64, no. 12, pp. 1626–1630, Dec. 1986.

[4] J. W. Meriwether, "A review of the photochemistry of selected nightglow emissions from the mesopause," *Journal of Geophysical Research: Atmospheres*, vol. 94, no. D12, pp. 14629–14646, 1989.

[5] T. G. Slanger and R. A. Copeland, "Energetic oxygen in the upper atmosphere and the laboratory," *Chemical Reviews*, vol. 103, no. 12, pp. 4731–4766, 2003.

[6] M. Kaufmann, F. Olschewski, K. Mantel, B. Solheim, G. Shepherd, M. Deiml, J. Liu, R. Song, Q. Chen, O. Wroblowski, D. Wei, Y. Zhu, F. Wagner, F. Loosen, D. Froehlich, T. Neubert, H. Rongen, P. Knieling, P. Toumpas, J. Shan, G. Tang, R. Koppmann, and M. Riese, "A highly miniaturized satellite payload based on a spatial heterodyne spectrometer for atmospheric temperature measurements in the mesosphere and lower thermosphere," *Atmospheric Measurement Techniques*, 11, 3861-3870, https://doi.org/10.5194/amt-11-3861-2018.

[7] P. Connes, " Spectromètre interférential à selection par l'amplitude de modulation" *J. Phys.Radium*, vol. 19 (3), pp. 215–222, 1958.

[8] J. M. Harlander and F. L. Roesler, "Spatial heterodyne spectroscopy: a novel interferometric technique for ground-based and space astronomy," *Proc.SPIE*, vol. 1235, 1990.

[9] N. G. Douglas, "Heterodyned holographic spectroscopy," *Publications of the Astronomical Society of the Pacific*, vol. 109, no. 732, p. 151, 1997.

[10] B. W. Smith and J. M. Harlander, "Imaging spatial heterodyne spectroscopy: theory and practice," *Proc.SPIE*, vol. 3698, 1999.

[11] S. Watchorn, F. L. Roesler, J. M. Harlander, K. P. Jaehnig, R. J. Reynolds, and W. T. Sanders, "Development of the spatial heterodyne spectrometer for vuv remote sensing of the interstellar medium," *Proc.SPIE*, vol. 4498, 2001.

[12] W. M. Harris, F. L. Roesler, J. Harlander, L. Ben-Jaffel, E. Mierkiewicz, J. Corliss, and R. J. Oliversen, "Applications of reflective spatial heterodyne spectroscopy to UV exploration in the solar system," *Proc.SPIE*, vol. 5488, 2004.

[13] F. L. Roesler, "An overview of the SHS technique and applications," in *Fourier Transform Spectroscopy/ Hyperspectral Imaging and Sounding of the Environment*. Optical Society of America, 2007.

[14] C. R. Englert, M. H. Stevens, D. E. Siskind, J. M. Harlander, and F. L. Roesler, "Spatial heterodyne imager for mesospheric radicals on STPSAT 1," *Journal of Geophysical Research: Atmospheres*, vol. 115, no. D20. [Online]. Available: https://agupubs.onlinelibrary.wiley.com/-doi/abs/10.1029/2010JD014398

[15] S. Watchorn, F. L. Roesler, J. Harlander, K. P. Jaehnig, R. J. Reynolds, and W. T. Sanders, "Evaluation of payload performance for a sounding rocket vacuum ultraviolet spatial heterodyne spectrometer to observe C IV 1550 emissions from the cygnus loop," *Appl. Opt., vol.* 49, *no.* 17, *pp.* 3265–3273, *Jun* 2010.

[16] A. E. Bourassa, J. Langille, B. Solheim, D. Degenstein, and F. Dupont, "The spatial heterodyne observations of water (SHOW) instrument for high resolution profiling in the upper troposphere and lower stratosphere," in *Light, Energy and the Environment*. Optical Society of America, 2016.

[17] M. Lenzner and J.-C. Diels, "Concerning the spatial heterodyne spectrometer," *Opt. Express*, vol. 24, no. 2, pp. 1829–1839, Jan 2016.

[18] J. M. Harlander, "Spatial Heterodyne Spectroscopy: Interferometric Performance at any Wavelength Without Scanning." Ph.D. dissertation, The University of Wisconsin - Madison., 1991.

[19] B. J. Cooke, B. W. Smith, B. E. Laubscher, P. V. Villeneuve, and S. D. Briles, "Analysis and system design framework for infrared spatial heterodyne spectrometers," *Proc.SPIE*, vol. 3701, 1999.

[20] J. Harlander, R. J. Reynolds, and F. L. Roesler, "Spatial heterodyne spectroscopy for the exploration of diffuse interstellar emission lines at far-ultraviolet wavelengths," *Astrophysical Journal, Part 1*, vol. 396, pp. 730–740, Sep. 1992.

[21] C. A. Barth and A. F. Hildebrandt, "The 5577 A airglow emission mechanism," *Journal of Geophysical Research*, vol. 66, no. 3, pp. 985–986, 1961.

[22] C. Barth, "Upper atmosphere three-body reactions study leading to light emission with laboratory results applied to night airglow," *NASA Technical Report*, no. 19650033531, 1964.

[23] M. Deiml, M. Kaufmann, P. Knieling, F. Olschewski, P. Toumpas, M. Langer, M. Ern, R. Koppmann, and M. Riese, "Dissect: development of a small satellite for climate research," *Proceedings of the 65th International Astronautical Congress, Toronto, Canada*, no. IAC-14,B5,1,10,x22911, 2014.

[24] M. Deiml, R. Song, D. Fröhlich, B. Rottland, F. Wagner, J. Liu, O. Wroblowski, Q. Chen, F. Loosen, M. Kaufmann, H. Rongen, T. Neubert, H. Schneider, F. Olschweski, P. Knieling, K. Mantel, B. Solheim, G. Shepherd, R. Koppmann, and M. Riese, "Test of a remote sensing fourier transform interferometer for temperature measurements in the mesosphere on a REXUS rocket," *Proceedings of the 23rd ESA Symposium on European Rocket and Balloon Programmes and Related Research, Visby, Sweden*, 2017.

[25] M. Kaufmann, M. Deiml, F. Olschewski, K. Mantel, F. Wagner, F. Loosen, D. FrÃ¶hlich, H. Rongen, T. Neubert, B. Rottland, H. Schneider, M. Riese, P. Knieling, J. Liu, R. Song, O. Wroblowski, Q. Chen, R. Koppmann, B. Solheim, J. Shan, and G. Shepherd, "A miniaturized satellite payload hosting a spatial heterodyne spectrometer for remote sensing of atmospheric temperature," *Proceedings of the 11th IAA Symposium on Small Satellites for Earth Observation, Berlin, Germany*, 2017.